materials

MDPI

Article

Effects of film thickness of ALD deposited Al_2O_3, ZrO_2 and HfO_2 nano-layers on the corrosion resistance of Ti(N,O) coated stainless steel

Mihaela Dinu[1], Kaiying Wang[2], Emile S. Massima Mouele[3], Anca C. Parau[1], Alina Vladescu[1,4], Xinhua Liang[2], Viorel Braic[1], Leslie Felicia Petrik[5] and Mariana Braic[1*]

[1] National Institute of Research and Development for Optoelectronics INOE 2000, 409 Atomistilor St., Magurele, Romania; mihaela.dinu@inoe.ro; anca.parau@inoe.ro; alinava@inoe.ro; viorel.braic@inoe.ro, mariana.braic@inoe.ro

[2] Department of Energy, Environmental & Chemical Engineering, Washington University in St. Louis, St. Louis, MO 63130, United States of America, kaiying@wustl.edu, Xinhua.Liang@wustl.edu

[3] Lappeenranta-Lahti University of Technology LUT, School of Engineering Science, Department of Separation Science, Yliopistonkatu 34, FI-53850 Lappeenranta, Finland, emile.massima@lut.fi

[4] Physical Materials Science and Composite Materials Centre, Research School of Chemistry & Applied Biomedical Sciences, National Research Tomsk Polytechnic University, Lenin Avenue 43, Tomsk, 634050, Russia; alinava@inoe.ro

[5] University of the Western Cape, Department of Chemistry, Environmental and Nano Sciences, Robert Sobukwe Road, Bellville, Republic of South Africa, lpetrik@uwc.ac.za

* Correspondence: mariana.braic@inoe.ro; Tel.: +40-(0)21-457-57-59.

Abstract: The goal of this work was to explore the potential of enhanced corrosion resistance of Ti(N,O) cathodic arc evaporation coated 304L stainless steel using oxide nano-layers deposited by atomic layer deposition (ALD). In this study, we deposited Al_2O_3, ZrO_2, and HfO_2 nano-layers with two different thicknesses by ALD onto Ti(N,O) coated 304L stainless steel surfaces. XRD, EDS, SEM, surface profilometry, and voltammetry investigation of the anti-corrosion properties of the coated samples were reported. The amorphous oxides nano-layers homogeneously deposited on the sample surfaces exhibited lower roughness after corrosion attack compared to the Ti(N,O) coated stainless steel. The best corrosion resistance was obtained for the thickest oxide layers. All samples coated with thicker oxide nano-layers augmented the corrosion resistance of the Ti(N,O) coated stainless steel in a saline, acidic, oxidising environment (0.9% NaCl + 6% H_2O_2, pH=4).

Keywords: atomic layer deposition; oxides; oxynitride; corrosion resistance

Citation: Dinu, M.; Wang, K.; Massima Mouele, E.S.; Parau, A.C.; Vladescu, A.; Xinhua Liang3; Braic, V.; Petrik, L.F.; Braic, M. **Effects of film thickness of ALD deposited Al_2O_3, ZrO_2 and HfO_2 nano-layers on the corrosion resistance of Ti(N,O) coated stainless steel.** *Materials* **2023**, *15*, x. https://doi.org/10.3390/xxxxx

Academic Editor(s):

Received: date
Accepted: date
Published: date

1. Introduction

The exposure of stainless steel (SS) to harsh environments may result in corrosion that further limits its performance and durability. It is necessary to develop an effective method to prevent corrosion. For decades, thin films have been studied because of their exceptional physical and chemical features including excellent thermal stability, low friction coefficient, and good wear resistance [1]. These properties have been improved by means of multilayers deposition onto the selected supports although their application depends on cost and practicality. Physical vapor deposition (PVP), such as the reactive arc evaporation process, has long been used as an adequate technique to develop monolayer and multilayer coatings. Titanium nitride (TiN) films obtained by PVD are claimed to show restricted corrosion protection ability due to their fundamental permeability. The increase of films thickness has been identified as a practical approach in order to enhance corrosion resistance [2]. Also, the use of bi- and multi- layered coatings containing two layers with distinct composition was productively used in engineering applications such

as automotive, aircraft or tool industries [1]. The superior features are the result of the presence of interfaces which ensure crack deflection, thus providing enhanced ductility, and decreased stress levels, resulting in higher adhesion to the bulk substrate. In corrosive environments the interfaces block the access of liquid to the bulk support, providing a superior corrosion resistance.

Subramanian et al. investigated the corrosion protection ability of titanium nitride coatings: TiN, TiON, and TiAlN for biomedical applications [3]. The TiN, TiON, and TiAlN films were deposited onto CP–Ti support by the DC reactive magnetron sputtering technique using two targets (Ti, Ti–Al) and a mixture of Ar and N_2. The corrosion resistance of CP–Ti support and TiN, TiAlN and TiON films was measured by potentiodynamic polarization and AC impedance experiments performed in simulated body fluid solution. Their results showed that CP–Ti /TiAlN coating exhibited higher corrosion performance~~. On the other hand, Chen et al. coated CoCrMo alloy with titanium oxide films prepared by the high power pulsed magnetron sputtering method [4]. The impact of Ti interlayer and thickness of Ti–O film on the film adhesion was examined. The corrosion resistance of plain CoCrMo alloy and CoCrMo/Ti–O coating was assessed by polarization tests. The results indicated that CoCrMo/Ti–O film exhibited excellent adhesion and demonstrated greater corrosion resistance compared to CoCrMo alloy support. An analogous study was conducted by Pruncu et al. who fabricated Zr, Nb and Si doped TiCN coatings onto stainless steel and Si wafer supports by the cathodic arc evaporation (CAE) method in a combination of N_2 and CH_4 gases [5]. Their results indicated that the engineered coating showed good adhesion, and the anticorrosion results revealed that TiNbCN had the best anti-corrosion properties in saline environments. The authors concluded that the TiNbCN coating was the most appropriate film to be used in harsh environments (high temperature, corrosive, etc.). In addition, various investigations on the coating of carbides, nitrides and oxynitrides and their durability on diverse supports have been demonstrated [6–8].~~ Ti(N,O) coatings represent a valuable choice due to their superior mechanical and tribological properties. The quite recent studies on titanium oxynitride films explored their dependency on the N/O ratio, which allow their use as solar selective absorbers [4=El-Fattah, H.A.A.; El-Mahallawi, I.S.; Shazly, M.H.; Khalifa, W.A. Optical properties and microstructure of TiNxOy and TiN thin films before and after annealing at different conditions. Coatings 9 (2019), 22, doi.org/10.3390/coatings9010022.], biocompatible materials [5=Rtimi, S.; Baghriche, O.; Sanjines, R.; Pulgarin, C.; Bensimon, M.; Kiwi, J. TiON and TiON-Ag sputtered surfaces leading to bacterial inactivation under indoor actinic light. J. Photochem. Photobiol. A Chem. 2013, 256, 52–63. doi.org/10.1016/j.jphotochem.2013.02.005] , [6=Subramanian, B.; Muraleedharan, C.V.; Ananthakumar, R.; Jayachandran, M. A comparative study of titanium nitride (TiN), titanium oxy nitride (TiON) and titanium aluminum nitride (TiAlN), as surface coatings for bio implants. Surf. Coat. Technol. 2011, 205, 5014–5020, doi.org/10.1016/j.surfcoat.2011.05.004], [7=Duta, O.C.; Ficai, D.; Ficai, A.; Andronescu, E.; Beshchasna, N.; Saqib, M.; Opitz, J.; Kraśkiewicz, H.; Wasyluk, Ł.; Kuzmin, O.; et al. Titanium oxynitride coatings deposited by magnetron sputtering for improvement of cardiovascular stent design. In Proceedings of the World Congress on New Technologies, Madrid, Spain, 19–21 August 2018; pp. 18–20., doi: 10.11159/icnfa18.112], plasmonic material for nanophotonics [8=Braic, L.; Vasilantonakis, N.; Mihai, A.; Garcia, I.J.V.; Fearn, S.; Zou, B.; Alford, N.M.; Doiron, B.; Oulton, R.F.; Maier, S.A.; et al. Titanium Oxynitride Thin Films with Tunable Double Epsilon-Near-Zero Behavior for Nanophotonic Applications. ACS Appl. Mater. Interfaces 2017, 9, 29857–29862, doi.org/10.1021/acsami.7b07660], or photocatalytic coatings [9=Asahi, R.; Morikawa, T.; Ohwaki, T.; Aoki, K.; Taga, Y. Visible-light photocatalysis in nitrogen-doped titanium oxides. Science 2001, 293, 269–271, DOI: 10.1126/science.1061051.], [10=Ahmed, M.; Xinxin, G. A review of metal oxynitrides for photocatalysis. Inorg. Chem. Front. 2016, 3, 578–590, DOI: 10.1039/C5QI00202H;], just to name a few. We previously reported on the improved corrosion resistance in 0.10 M NaCl + 1.96 M H_2O_2 solution of the cathodic arc deposited TiNO coating, with low oxygen concentration

(about 7.3 at.%), compared to TiN coating obtained by the same deposition method [38]. Even if TiN coatings are known to be corrosion resistant, Esaka et al. demonstrated by absorption and X-ray photoelectron spectroscopies that the oxidation of TiN films in an oxidizing environment is ascribable to the formation of Nx-Ti-Oy like structures, permitting the diffusion of oxygen from the corrosive solution, and so is observed a decrease of the corrosion resistance of TiN compared to CrN, in which Cr_2O_3 is immediately formed at the coating – solution interface , without formation of a Nx-Cr-Oy like structures [11=Esaka, F.; Furuya, K.; Shimada, H.; Imamura, M.; Matsubayashi, N.; Sato, H,; Nishijima, A.; Kawana, A.; Ichimura, H.; Kikuchi, T., Journal of Vacuum Science &Technology a-Vacuum Surfaces and Films 15 (1997) 2521–2528, doi: 10.1116/1.580764]. Attempting to further improve the corrosion resistance of Ti(N,O) coatings with low oxygen content, we consider to apply a second layer of ultrathin oxide coating, due to the known good chemical and mechanical stability of oxide films [12=Li, M.; Jin, Z-X.; Zhang, W.; Bai, Y-H.; Cao, Y-Q.; Li, W-M.; Wu, D.; Li A-D., Comparison of chemical stability and corrosion resistance of group IV metal oxide films formed by thermal and plasma-enhanced atomic layer deposition, Scientific Reports 9 (2019) 10438, doi: 10.1038/s41598-019-47049-z]. Because TiN and Ti(N,O) grown by cathodic arc evaporation present a compressive stress, we chose to use a deposition method which may produce a very thin, continuous and conformal coating to avoid delamination of the two layers. ~~However, increasing the corrosion protection of bulk metallic alloys remains a challenge. Therefore, it is crucial to explore new methods using nano layered materials either as pre-treatment or as top coating technique. Apart from thick coatings, ultrathin ceramic coatings can be a good choice for protecting metal surfaces due to the good chemical and mechanical stability of ceramic films~~. These dense and conformal films are expected to diminish the pinhole density specific for the cathodic arc evaporation deposited coatings, enabling sealing even with thin coatings of nanometer thicknesses [13=9].

Even though various approaches have been used to prepare thin films, it is still challenging to obtain a smooth and conformal dense film. Previous investigations claimed that ALD is an advanced method to engineer films of good quality at the nanoscale [14,15=10,11]. Atomic layer deposition (ALD) is a self-limiting reaction that involves the use of a precursor and oxidant followed by a flow of inert gas [16,17=12,13]. The common advantages of ALD include the control of film thickness, minor structural pinholes, low defect density, and good film uniformity [18-19=14,15]. These unique properties justify the extensive application of ALD for film coatings over the past decades [20-24=16-20]. M. Fedel and F. Deflorian performed atomic layer deposited Al_2O_3 films on AISI 316L stainless steel [25=21]. The corrosion resistance of Al_2O_3 deposits were evaluated by potentiodynamic measurements and electrochemical impedance spectroscopy (EIS) in 0.2 M NaCl saline environment for up to 1000 hours of non-stop immersion. Their outcomes showed that the corrosion current density of the bare support (10^{-6}A/cm^2) declined proportionally with the increase of deposition layers Al_2O_3–500 (10^{-8}A/cm^2) and Al_2O_3–1000 (10^{-9}A/cm^2), respectively. Their results suggested that the addition of Al_2O_3 layers greatly shielded the bare AISI 316L stainless steel against corrosive aggression. Therefore, increasing the number of ALD cycles increased the film thickness and gave better corrosion protection. Belén Díaz et al. engineered ultra-thin (5 to 50 nm) films of aluminum and tantalum oxides by ALD onto a 316L stainless steel support [26=22]. The corrosion protection behavior of the coatings was investigated by linear scan voltammetry (LSV), and electrochemical impedance spectroscopy (EIS) in 0.8 M NaCl saline medium. The effects of the deposition temperature (250 °C and 160 °C) and coating thickness were examined. The polarization results indicated that the current density decreased by up to four orders of magnitude with an increase of coating thickness from 5 to 50 nm. In both cases, thicker coatings (50 nm) of Al_2O_3 and Ta_2O_5 exhibited the greatest corrosion resistance at 250 °C with Al_2O_3 having superior shielding properties. These examples show that ALD is an ideal method because it is capable of depositing ultrathin, conformal films with sub-nanometre thickness control [27=23]. ALD has been widely used in anti-corrosion applications without diminishing the

desirable functions of the support [13, 27-29=9, 23-25]. Generally, inorganic coatings, especially ceramics, show good insulating, tribological, and corrosion resistance properties in aggressive media. Al_2O_3 is the most frequently studied ALD thin film for corrosion protection, because it has been shown to nucleate well on metals giving rise to low porosity that prevents the solution from accessing the metal [27, 30, 31=23, 26, 27]. ZrO_2 reveals excellent properties such as high strength, high fracture toughness, excellent wear resistance, high hardness, and excellent chemical resistance [32-36=28-32]. HfO_2 is a highly resistive material; its dielectric constant is several times higher than conventional silica gate dielectrics. The Pourbaix diagram shows the formation of a stable passive oxide on hafnium over the entire potential pH range. Due to these features, thin layers of HfO_2 are applied for anticorrosion protection [35,36=31,32].

Suk Won Park et al. deposited alumina as a corrosion protective wear onto silver particles by ALD [37=33]. The corrosion resistance of the coatings was evaluated in an artificial sweat solution at 25 and 35 °C for 24 h. The effect of layers thickness (varied from 20 to 80 nm) on their corrosion protection ability was also investigated. Their results indicate that thick layers of ALD alumina robustly protected the shape and light reflectance of the sputtered silver particles, while the bare silver specimen was aggressively attacked by the simulated body fluid. Similar ALD investigations for corrosion protection of different substrates have been reported [38-41=34-37].

However, despite these studies, there is insufficient research on the improvement of corrosion resistant of Ti(N,O) film by ALD coating of ceramic layers. In this study, we coated Al_2O_3, ZrO_2, and HfO_2 thin films of various thicknesses on stainless steel support surfaces by ALD to investigate their anti-corrosion performance. We theorize that Al_2O_3, ZrO_2 and HfO_2 prepared by ALD could improve the corrosion protection properties of the Ti(N,O) coating that we previously developed by CAE onto stainless steel support [42=38]. Based on our information the deposition on stainless steel supports of different layers obtained by CAE and then by ALD was not reported till now. The rational of this approach is based on the attempt to combine the chemical stability of oxide films obtained by ALD which are perfectly enrobing the support, and the high hardness and adhesion of the coatings synthesized by CAE. Furthermore, we used an accelerated corrosion test using saline~~,~~ ~~acidic~~ and oxidizing solution. To our knowledge there are few examples of ~~such~~ tests carried out in such corrosive solution [43-45=39-41] carried out on ALD coated ~~metallic~~ supports. The corrosion protection behavior of the fabricated coatings was assessed by potentiodynamic polarization tests in simulated corrosive environment (0.9% NaCl + 6% H_2O_2, pH=4). The effect of the number of ALD cycles on ceramic film thickness and corrosion resistance were also investigated.

2. Materials and Methods

All coatings were deposited on 304L stainless steel, abbreviated in the following as SS. The composition of 304 SS rods, provided by Bibus Metals AG, Fehraltorf, Switzerland), from which the discs were machined, is (wt.%): Fe = 70.974%, Cr = 17.742%, Ni = 8.526%, Mn = 1.23%, Mo = 0.585%, Cu = 0.536%, Si = 0.206%, Co = 0.16%, P = 0.021%, S = 0.014%, and C = 0.006%.

2.1. Coatings Deposition

According to a previous study [4=38], PVD deposited Ti(O,N) showed the highest protection efficiency for SS against NaCl corrosive attack.

To summarize, the Ti(N,O) coatings were deposited on SS discs (20 mm diameter and 2 mm thickness) using a Ti cathode (99.5% purity, Cathay Advanced Materials Ltd., Guangzhou, China) by reactive CAE in a mixture of nitrogen and oxygen. We chose 304L SS because compared to other types of stainless steels, it has a low carbon content, such that it presents a higher corrosion resistance. Also, it is non-magnetic after annealing, which might be of interest for certain applications.

The discs were first polished with abrasive paper (80 to 800 mesh size) and then repeatedly with 0.5 μm diamond suspension to reach a roughness (R_a) of about 13 nm. The discs were cleaned using an ultrasonic bath in acetone, isopropyl alcohol and lastly in distilled water, and then were flushed with dried nitrogen. After being introduced in the deposition chamber, on a rotating holder which ensured the coating uniformity, a residual pressure of 5×10^{-4} Pa was attained. Then the discs were bombarded by 1 keV Ar^+ at 10^{-2} Pa for final cleaning. The Ti(N,O) deposition parameters were as follows: total gas pressure during deposition = 8×10^{-2} Pa; N_2 flow rate = 60 sccm; O_2 flow rate = 17 sccm; arc current on Ti cathode = 90 A; support bias voltage = −200 V; support temperature = 200 °C. All the 21 SS discs were coated with Ti(N,O) in one run, due to the large diameter of the deposition chamber (80 cm).

In the present work, ALD was employed to further inhibit corrosion of the prepared SS/Ti(N,O) by Al_2O_3, ZrO_2 and HfO_2 layers deposition. Precursors were trimethylaluminum (TMA, Sigma Aldrich) and deionized (DI) water for Al_2O_3 ALD, tetrakis(dimethylamido)zirconium (TDMAZ, Sigma Aldrich) and 30 wt.% hydrogen peroxide (Sigma Aldrich) in water for ZrO_2 ALD, and tetrakis(diethylamido)hafnium (TDEAH, Sigma Aldrich) and 30 wt.% hydrogen peroxide in water for HfO_2 ALD.

For the Al_2O_3 ALD, 40 and 80 cycles of Al_2O_3 ALD (40c- and 80c- Al_2O_3) were applied; for the ZrO_2 ALD, 45 and 90 cycles of ZrO_2 ALD were applied; and for the HfO_2 ALD, 55 and 110 cycles of HfO_2 ALD were applied. Each type of oxide coating with two thickness was deposited on three SS/Ti(N,O) samples.

In a typical run, the pieces of SS/Ti(N,O) were degassed at 150 °C overnight under nitrogen (N_2) atmosphere before ALD. All the ALD processes were carried out at 200 °C. All precursor feed lines were kept above 120°C to prevent the condensation of any precursors. Taking Al_2O_3 ALD as an example, TMA was used as the Al precursor and DI water as the other reactant. TMA was kept at 25 °C to achieve a reasonable vapor pressure. The obtained TMA vapor was carried by ultrahigh purity N_2 to the reactor. Then, the system was held for several seconds. After that, unreacted precursors and any byproducts were removed by ultrahigh purity N_2 during the reaction. The timing sequence for a typical Al_2O_3 ALD was 5 s, 10 s, 180 s, 30 s, 3 s, 10 s, 180 s, and 30 s for TMA dose, system hold, N_2 flush, evacuation, DI water dose, system hold, N_2 flush, and evacuation, respectively. ZrO_2 and HfO_2 ALD followed a similar procedure. The temperature for the TDMAZ/TDEAH bubbler was held at 80°C. The time sequence for ZrO_2 and HfO_2 ALD was 10 s, 20 s, 240 s, 30 s, 5 s, 20 s, 240 s, and 30 s for TDMAZ/TDEAH dose, system hold, N_2 flush, evacuation, 30 wt.% hydrogen peroxide dose, system hold, N_2 flush, and evacuation, respectively. In the ALD process the number of cycles was chosen so as to obtain the same thickness values for all oxides, i.e. 5 nm for the lower number of cycles and 10 nm for the highest ones. This choice of metal oxide was based on our previous studies [46=42]. The number of cycles was determined based on different theoretical growth rate. For example, Al_2O_3 exhibited a growth rate of 1.3Å per cycle [47=43], while ZrO_2 was 1.2Å per cycle [48=44], slightly lower than that of Al_2O_3. HfO_2 had a growth rate of 0.94 Å per cycle [49=45].

2.2. Coatings Characterization

A Dektak 150 surface profilometer (Bruker, Billerica, MA, USA) - 2.5 μm stylus diameter, was used to measure the Ti(N,O) coatings and the surface roughness of the SS supports as well as all the deposited coatings.

All roughness measurements were done in randomly chosen 10 areas, the results being averaged. The roughness of each coating was determined over 1 cm during 200 s. Three roughness parameters were used for roughness evaluation and their impact on corrosion resistance: Ra (arithmetic average), Rq (root-mean square), and Sk (symmetry of the profile about the mean line).

A Hitachi TM3030 Plus (Tokyo, Japan) scanning electron microscope (SEM) coupled to an energy dispersive X-ray spectrometer (EDS) (Bruker, Billerica, MA, USA) provided

the surface morphology and elemental composition of the coatings. The elemental composition measurements were done in three different areas on each deposited coating, the results were averaged, and the standard deviation (SD) was calculated. The images of surface morphology and elemental composition were obtained by mixed images of backscattering and secondary electrons in one area.

A SmartLab diffractometer (Rigaku, Tokyo, Japan) with CuK$_\alpha$ radiation (λ = 0.15405 nm) was used for phase composition investigation. The measurements were performed in a 2θ range of 20° to 100°, using the following parameters: 2° incidence angle, 2°/min. scanning speed, 0.02° step size.

The corrosion process was evaluated by a potentiostat/galvanostat VersaSTAT 3 (Princeton Applied Research, Oak Ridge, TN, USA) and the data were recorded using Versa Studio software (version 2.60.6, Princeton Applied Research, Oak Ridge, TN, USA). 100 ml of 0.1 M NaCl + H_2O_2 (pH = 4) was used as test medium. Th tests were carried out at room temperature (22 ± 1°C). A three standard electrode cell was used, with platinum as the counter electrode (CE), Ag/AgCl (KCl sat. (0.197 V)) as the reference electrode (RE) and the investigated specimens as the working electrode (WE) (mounted in a Teflon holder with 1 cm^2 exposed area). After immersion, the specimens were monitored for 1 h, while the open circuit potential (E_{oc}) was recorded over time. The corrosion potential (E_{corr}), corrosion current density (i_{corr}), anodic (β_a) and cathodic (β_c) slopes were directly estimated from Tafel plots, which were recorded from - 250 to 250 mV vs. E_{oc}, at a scanning rate of 1 mV/s. Polarization resistance (R_P) was calculated based on Stern–Geary equation [50=46], using the i_{corr} values previously determined, and Tafel anodic and cathodic slopes.

The samples designation indicates the support (SS), the first coating Ti(N,O) deposited by reactive CAE, and the second layer of oxide deposited by ALD along with the number of cycles, e.g. SS/Ti(N,O)/Al_2O_3-40c.

3. Results

3.1. Surface morphology and elemental composition

Table 1 presents the elemental composition of the samples. The acquisition time for the EDS analysis was chosen according to films thickness: 1200 s for Ti(N,O) coatings – about 1 μm thick, and 3600 s. for the other 6 oxynitride/oxide coatings.

Table 1. Elemental composition of the investigated specimens.

Sample	Al (at. %)	Zr (at.%)	Hf (at.%)	O (at.%)	Ti (at.%)	N (at.%)	Fe (at.%)
SS/Ti(N,O)	-	-	-	8.95±0.53	52.60±2.28	47.58±1.72	0.87±0.07
SS/Ti(N,O)-Al_2O_3-40c	1.802±0.106			28.13±1.72	41.61±2.09	27.36±1.44	1.09±0.09
SS/Ti(N,O)-Al_2O_3-80c	2.887±0.165			37.29±2.43	37.11±2.25	21.82±1.25	0.89±0.082
SS/Ti(N,O)-ZrO_2-45c		0.710±0.102		23.18±1.28	48.06±2.14	26.77±1.26	1.288±0.09
SS/Ti(N,O)-ZrO_2-90c		1.832±0.230		37.70±2.10	44.28±2.49	15.05±0.75	1.14±0.09
SS/Ti(N,O)-HfO_2-55c			0.006±0.001	8.05±0.49	50.85±2.18	39.70±1.80	1.40±0.10
SS/Ti(N,O)-HfO_2-110c			0.540±0.127	17.06±1.01	47.99±2.17	33.06±1.60	1.36±0.10

Figures 1 to 4 show the surface morphology of all coatings. It is noticeable that the few visible pinholes on SS/Ti(N,O) sample disappeared after ALD coating. The EDS results for each coating, also shown in Figures 1 – 4, indicate the homogenous distribution

of elements on each sample's surface, as observed on both images, displaying only the oxides elements (left) and all the elements (right). The presence of each metal in the ALD deposited oxides is well visible, including some small metal agglomeration. This comes from the ultrathin nature of ALD. All the coatings are thin enough that EDS can still clearly detect the metal composition under the coatings. One can observe that the signal corresponding to atomic Fe concentration increased in the case of SS/Ti(N,O)-HfO_2 coatings, indicating that the bilayers were thinner than the other types of ALD coatings, probably due to slow growth rate of HfO_2. The actual thickness of HfO_2 may be thinner than expected. The designed thickness of HfO_2 was estimated from literature. However, the actual growth rate varied because of different conditions such as dose time and different substrates. The reported growth rate was an average value based on several hundred cycles. The initial growth rate may be slower than the average value. Unlike Al_2O_3 and ZrO_2, HfO_2 followed an island growth mechanism: nucleation, development of separated nuclei and flattening. So, 55 cycles of HfO_2 may not be enough for a smooth film. Therefore, 110 cycles of HfO_2 was required to protect the substrate.

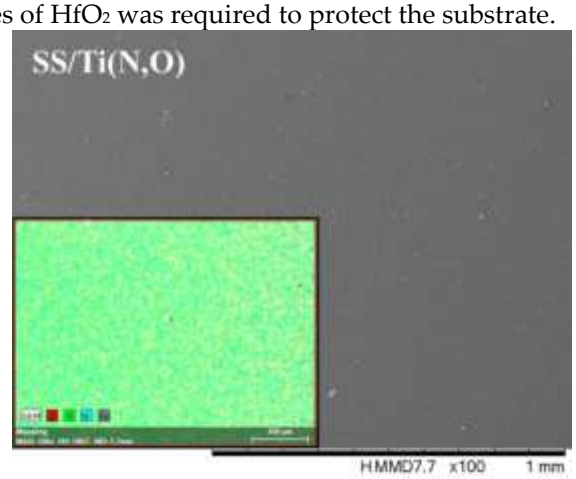

Figure 1. SEM micrographs (x100) and elemental distribution of SS/T(N,O) layer.

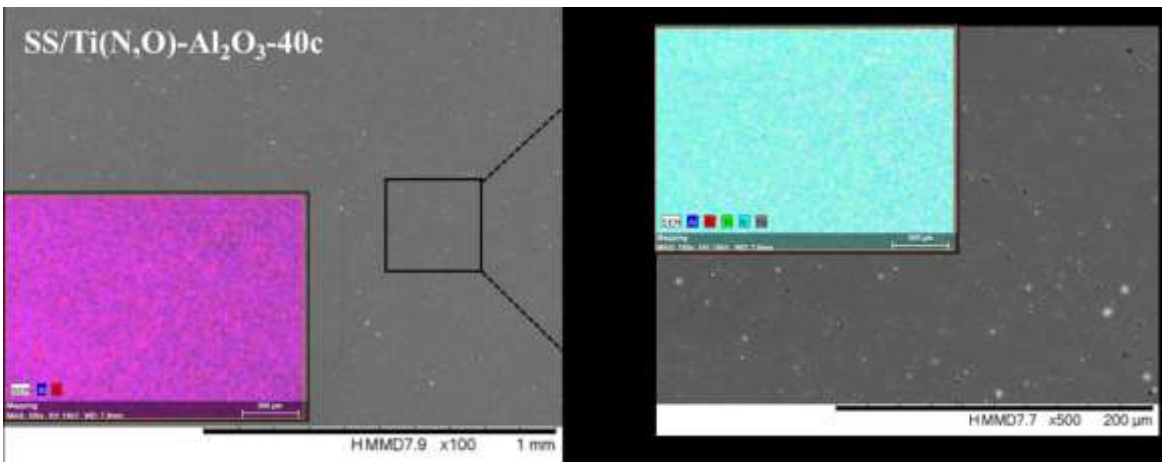

(x100) *a)* *(x500; x100 in inset)*

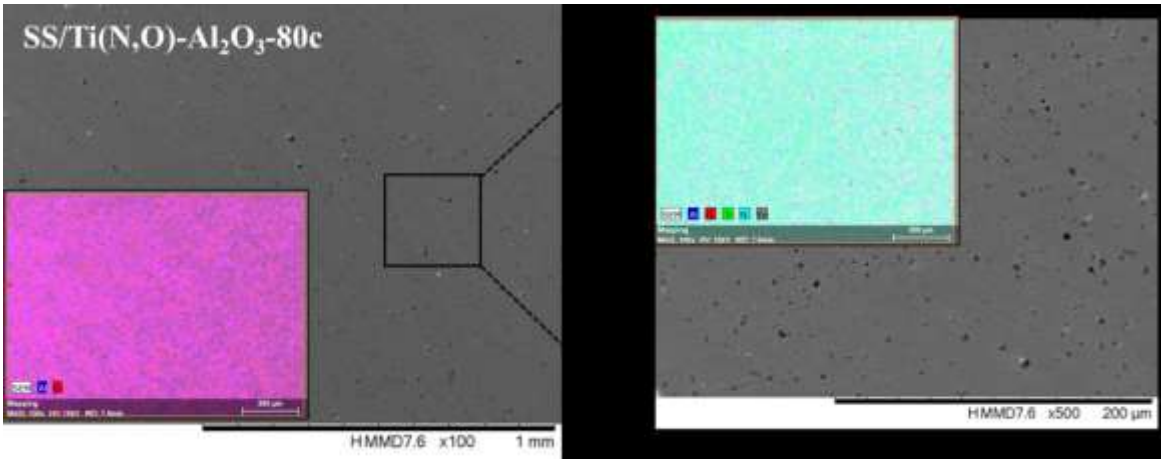

(x100) *b)* *(x500; x100 in inset)*

Figure 2. SEM micrographs and (Al and O) distribution of Al_2O_3 layer coated with a) 40 cycles and b) 80 cycles.

308

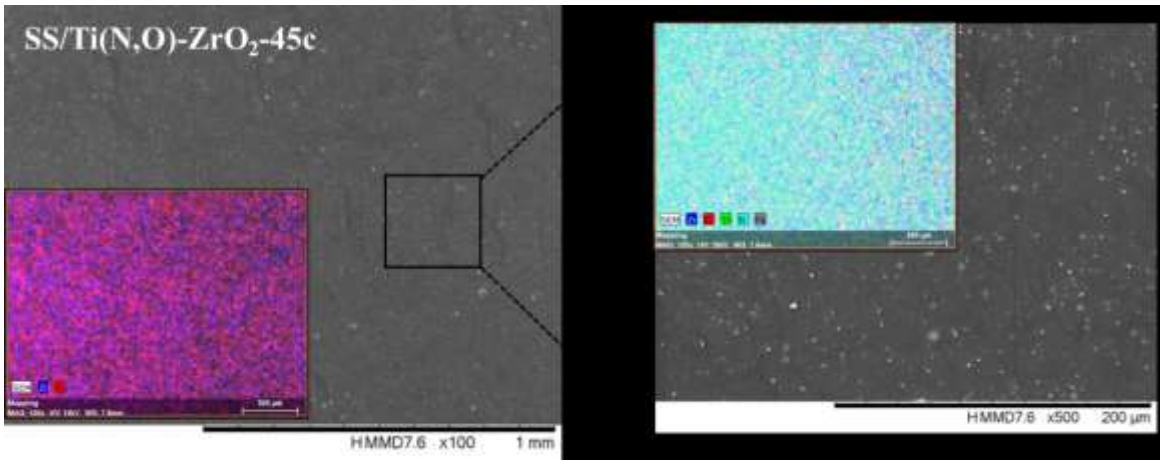

(x100) *a)* *(x500; x100 in inset)*

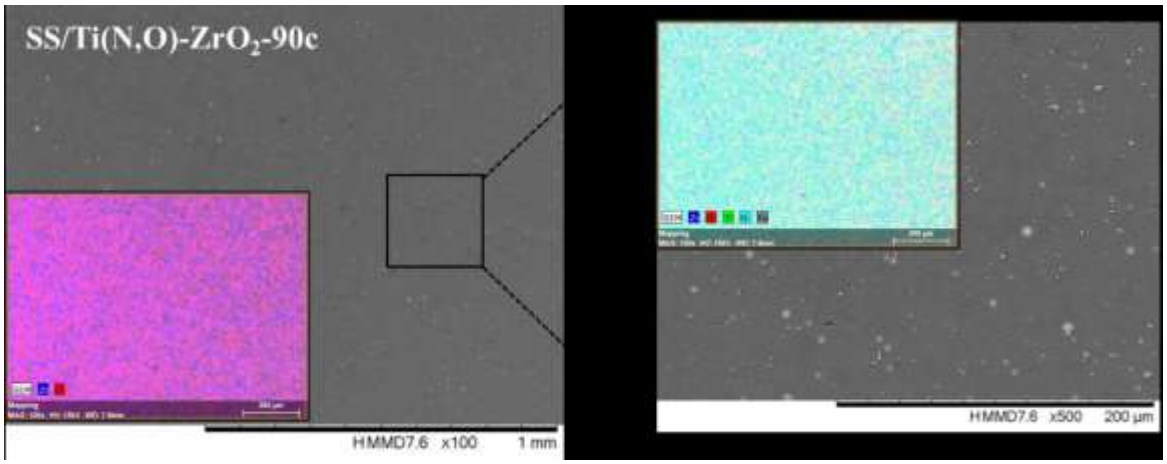

(x100) *b)* *(x500; x100 in inset)*

Figure 3. SEM micrographs and (Zr and O) distribution of ZrO_2 layer coated with a) 45 cycles and b) 90 cycles.

309

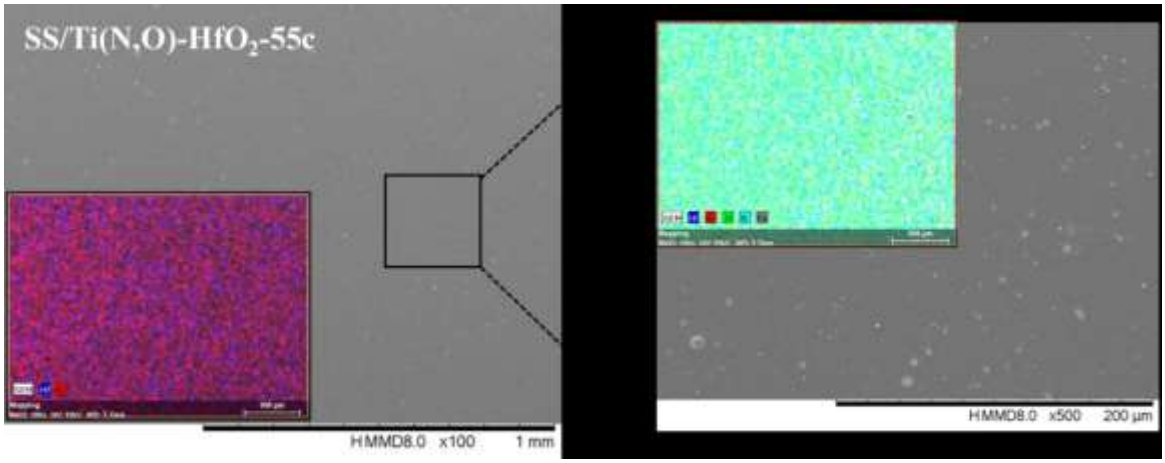

(x100) *a)* *(x500; x100 in inset)*

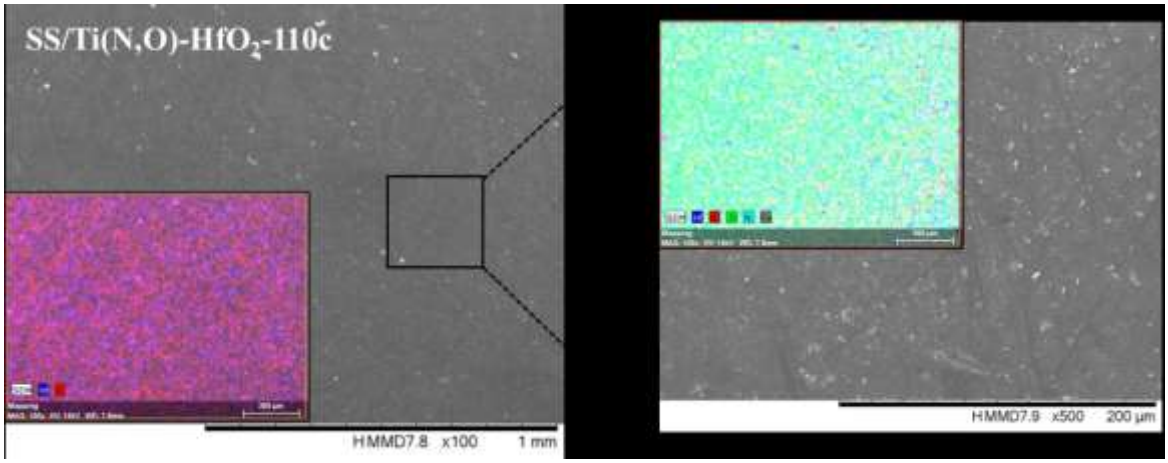

(x100) *b)* *(x500; x100 in inset)*

Figure 4. SEM micrographs and (Hf and O) distribution of HfO_2 layer coated with a) 45 cycles and b) 90 cycles.

310

3.2. Phase Composition

311

The diffractograms show the maxima specific for the SS support and for the Ti(N,O) coatings. Even if the ALD deposited layer showed no specific signature, it is clear that the ALD process had a certain influence on the SS support, as the support and Ti(N,O) maxima have lower intensity values. The ALD temperature was 200 ºC, which is not high enough to crystallize in general. For example, ZrO_2 starts to crystallize at 420 ºC [51=47].

312 313 314 315 316

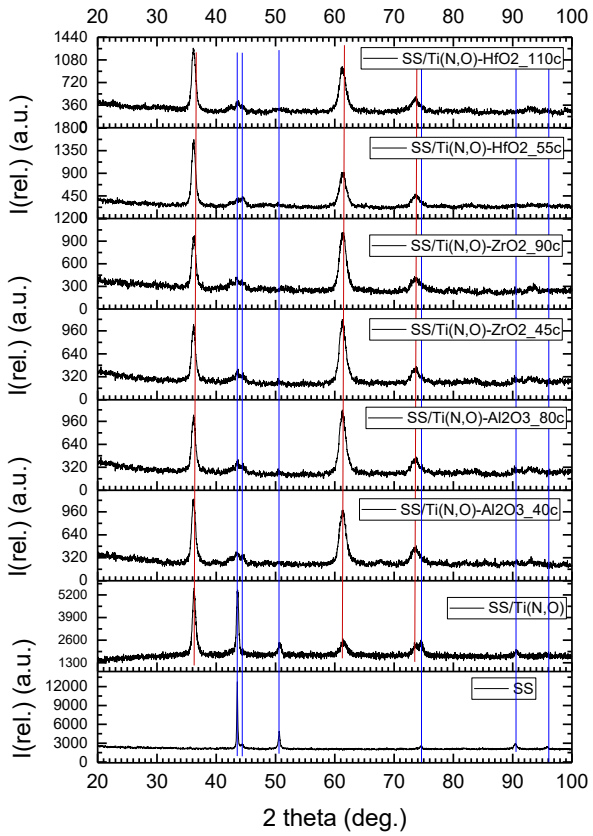

Figure 5. Diffractograms of the 304 L support (SS), the Ti(N,O) coating and ALD deposited thin films.

The as-deposited HfO_2 films were amorphous and remained amorphous after annealing at 400 and 450 °C. At an annealing temperature higher than 500 °C, diffraction peaks appeared, indicating the formation of crystalline HfO_2 [52=48]. For a flat support, the amorphous Al_2O_3 phase of any thickness was always the most stable in the case of ALD deposition [53, 54=49, 50].

3.3. Surface roughness before and after the corrosive attack

Figures 6 – 8 show the main roughness parameters of the coatings before and after the corrosion attack. The roughness of all samples increased significantly after the corrosion tests. The most significant increase of the Ra and Rq parameters was noted for the SS and SS/Ti(N,O) sample, while in the case of the oxide coated samples just a slight increase was observed. Before corrosion, in contrast to the SS and SS/Ti(N,O) samples, the oxide coated samples exhibited not only higher roughness values, but also a large dispersion of the measured value.

Due to the quite large non-uniformities present on the surfaces, the roughness parameters of the oxide coated samples are in the same range, such that surface roughness could not be further used in the assessment of corrosion resistance.

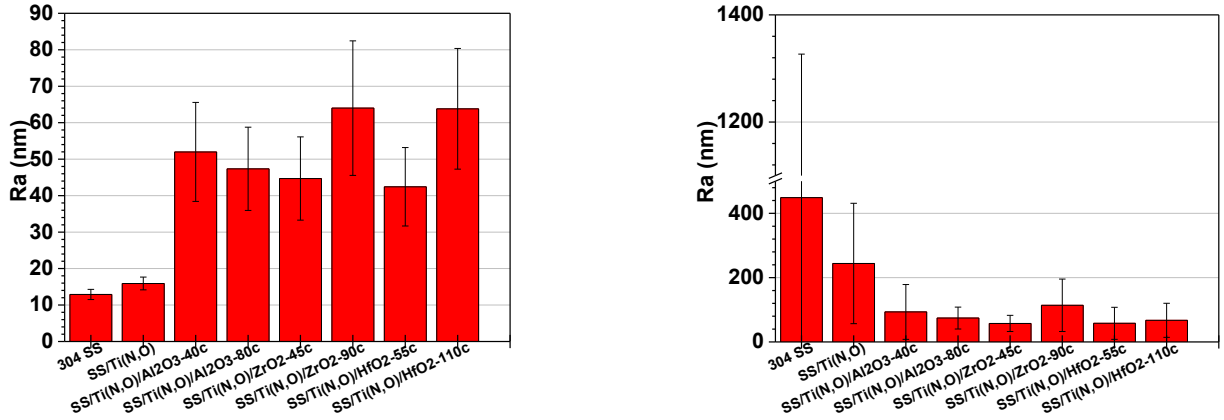

a *b*

Figure 6. Ra roughness parameter of the samples: a) before and b) after the corrosion tests.

337

338

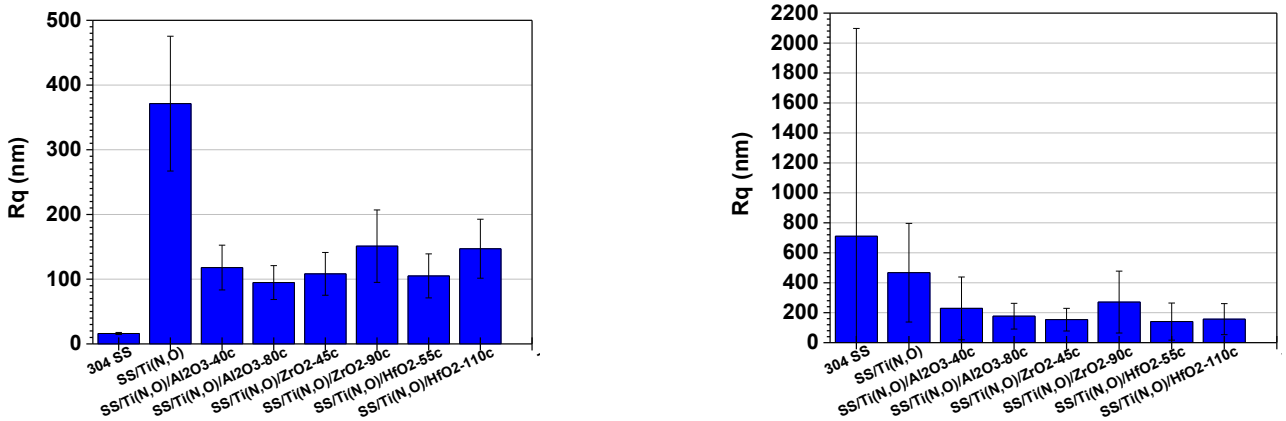

a *b*

Figure 7. Rq roughness parameter of the samples: a) before and b) after the corrosion tests.

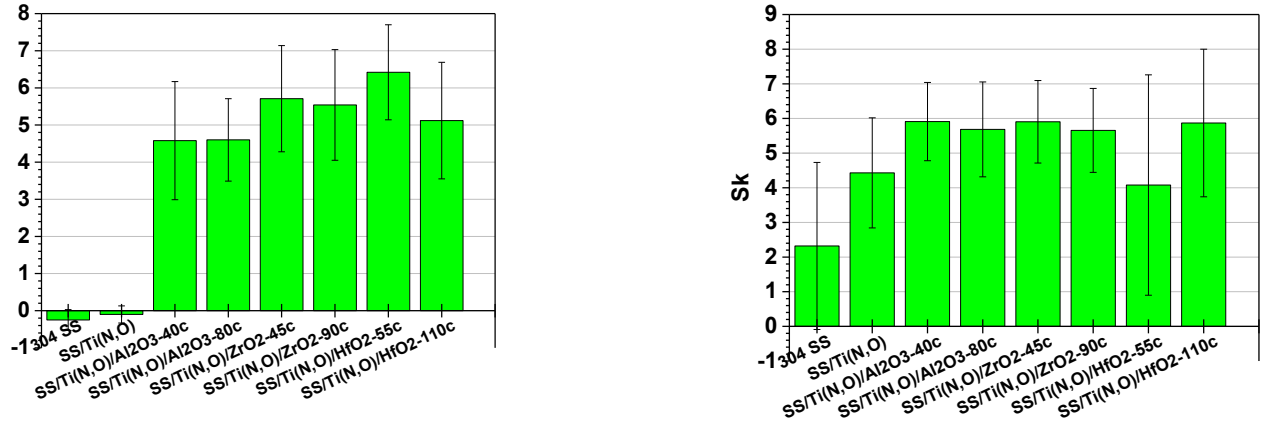

a b

Figure 8. Sk roughness parameter of the samples: a) before and b) after the corrosion tests.

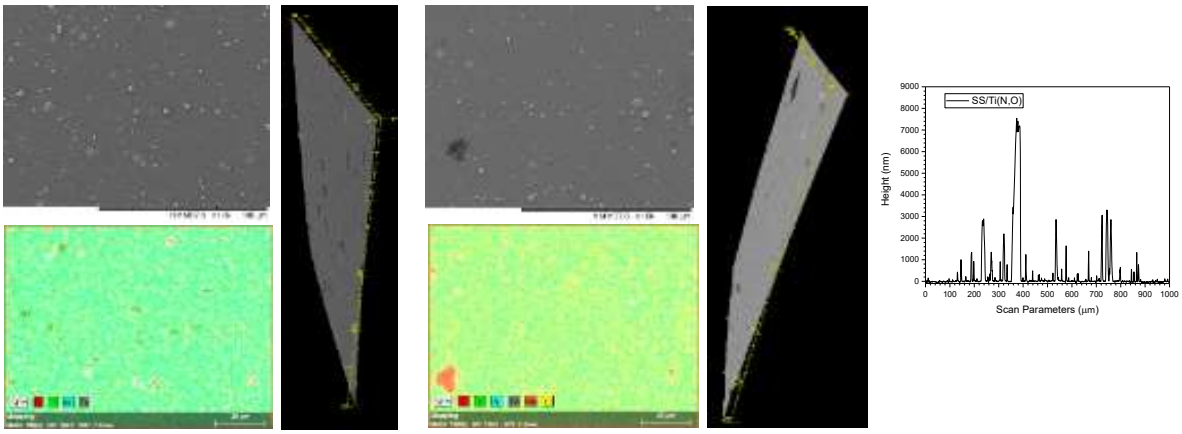

a b c

Figure 9. SS/Ti(N,O) surface morphology: 2D and 3D SEM images (x1000) and related EDS image a) before corrosion, b) after corrosion, c) scanned line on the surface after corrosion.

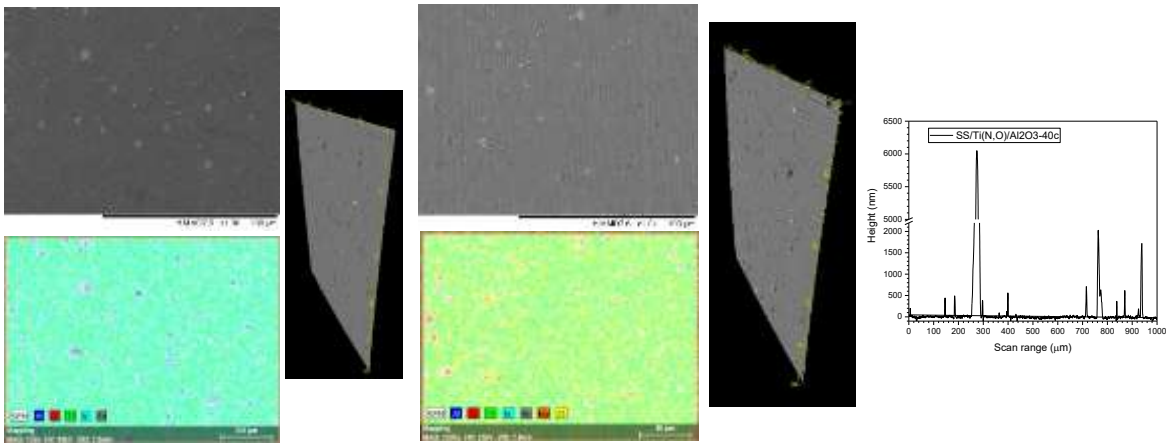

a B c

Figure 10. SS/Ti(N,O)/Al2O3-40c surface morphology: 2D and 3D SEM images (x1000) and related EDS image a) before corrosion, b) after corrosion, c) scanned line on the surface after corrosion.

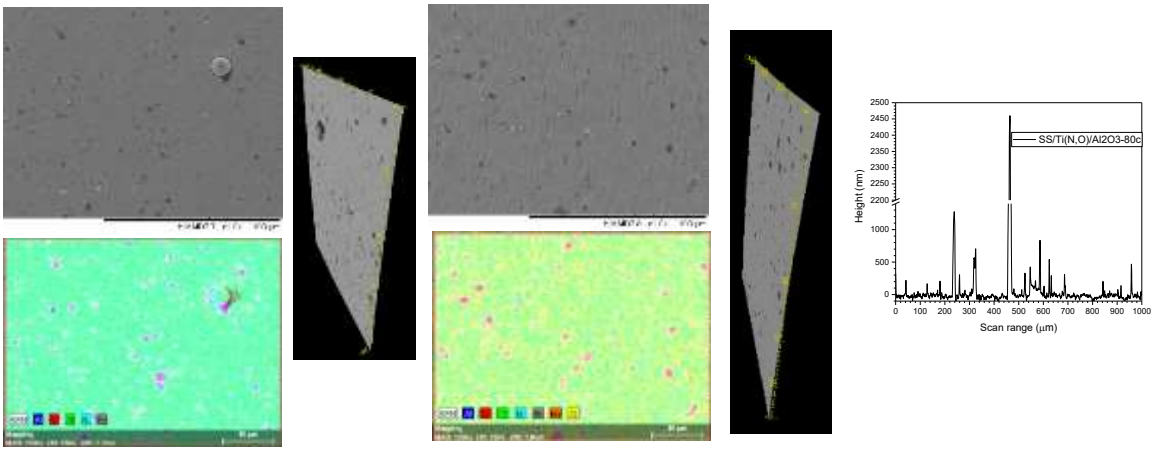

a b c

Figure 11. SS/Ti(N,O)/Al2O3-80c surface morphology: 2D and 3D SEM images (x1000) and related EDS image a) before corrosion, b) after corrosion, c) scanned line on the surface after corrosion.

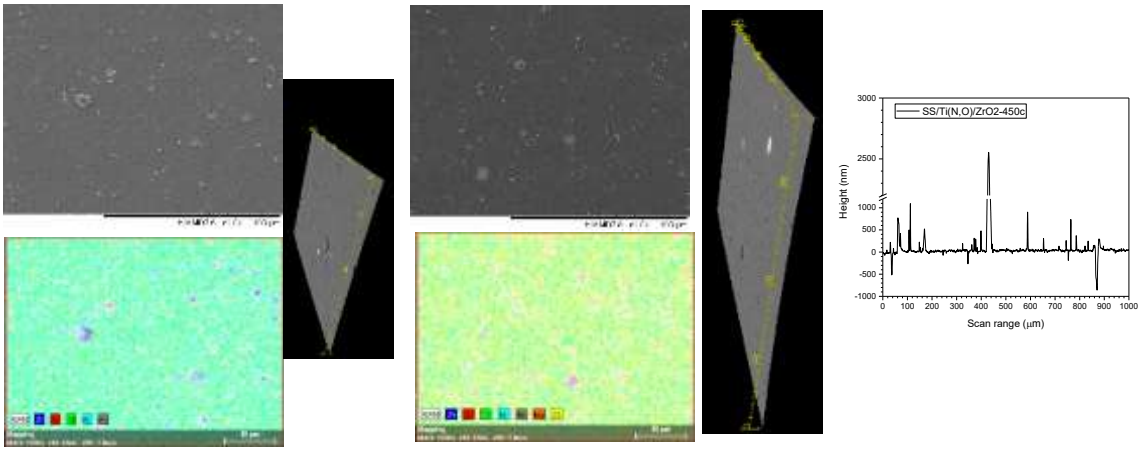

a b c

Figure 12. SS/Ti(N,O)/ZrO_2-45c surface morphology: 2D and 3D SEM image (x1000) and related EDS image a) before corrosion, b) after corrosion, c) scanned line on the surface after corrosion.

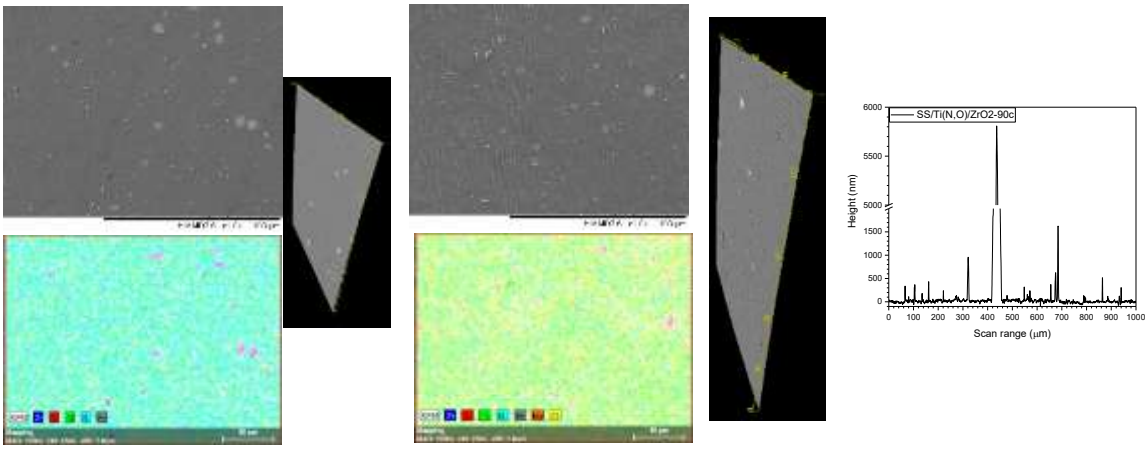

a b c

Figure 13. SS/Ti(N,O)/ZrO_2-90c surface morphology: 2D and 3D SEM images (x1000) and related EDS image a) before corrosion, b) after corrosion, c) scanned line on the surface after corrosion.

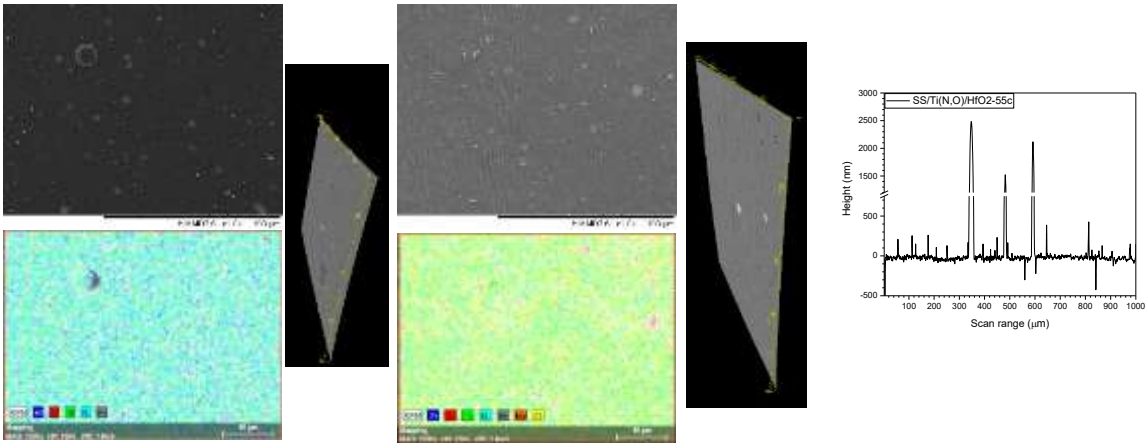

a *b* *c*

Figure 14. SS/Ti(N,O)/HfO_2-55c surface morphology: 2D and 3D SEM images (x1000) and related EDS image a) before corrosion, b) after corrosion, c) scanned line on the surface after corrosion.

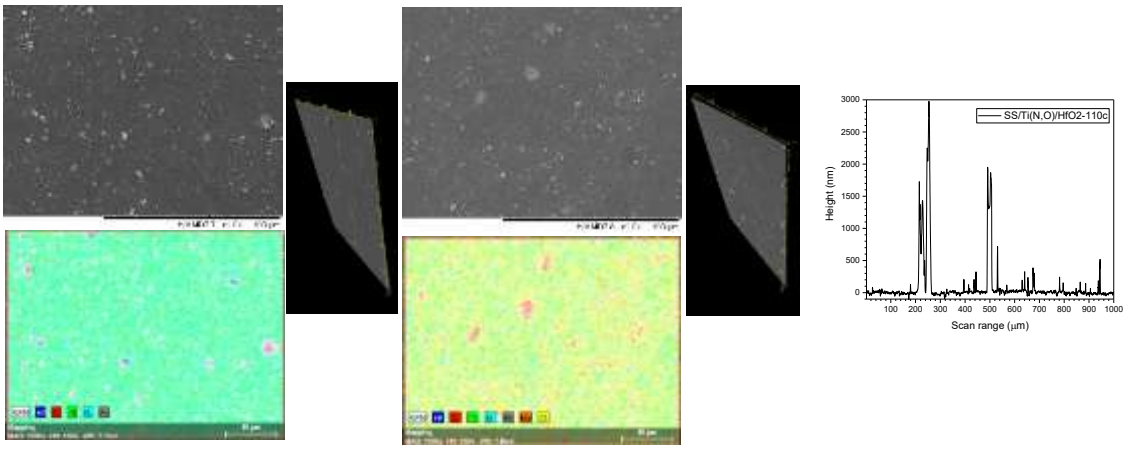

a *b* *c*

Figure 15. SS/Ti(N,O)/HfO_2-110c surface morphology: 2D and 3D SEM image (x1000) and related EDS image a) before corrosion, b) after corrosion, c) scanned line on the surface after corrosion.

To sustain this statement, Figures 9 – 15 present the morphology of coated sample surfaces, as SEM 2D and 3D images, EDS images before and after corrosion tests, along with an example of the scanned line on their corroded surfaces showing in detail the surface features responsible for the large error bars. The corroded surface showed traces of the solution used as electrolyte, as seen in the EDS images.

3.4. Electrochemical evaluation - Tafel plots

The results obtained from the corrosion tests are presented in Table 2. Considering the Tafel plots (Figure 16), one can see that both the uncoated and Ti(N,O) coated SS showed a local disruption of the passive layer, evidenced by the breakdown potential (E_b), giving rise to a sharp increase of the ion current density, indicating that local corrosion processes were activated. The E_b(SS/Ti(N,O) is located at about 405 mV while E_b(SS) is located at 221 mV, indicating that in the bare SS metal the cathodic process was significantly higher than in the coated one. No breakdown was observed in the case of samples with top nano-layer of Al_2O_3 and ZrO_2. However, SS/Ti(N,O)/HfO_2 coatings presented two breakdown values, for both thickness values. Also, the position of both breakdown potentials related to SS/Ti(N,O)/HfO_2-55c coating were lower than the one related to SS/Ti(N,O).

The Tafel slopes (βc and βa) were determined from the parts which exhibited linearity in accordance with the Tafel relationship. The calculated values of the cathode and anode slope were all high. However, for the bare SS support the cathodic slope was significantly higher than the anodic one, indicating a cathodic reduction detrimental to the anodic oxidation. In the case of SS/Ti(N,O) coatings the slopes were quite similar, such that it may be concluded that the hydrogen evolution and metal dissolution were almost in equilibrium. For the ALD coated samples, except for SS/Ti(N,O)/HfO_2-110c, the anodic slope became higher than the cathodic slope, indicating an inhibition action of the oxides by simply blocking the metal from interaction with the acidic and oxidizing environment.

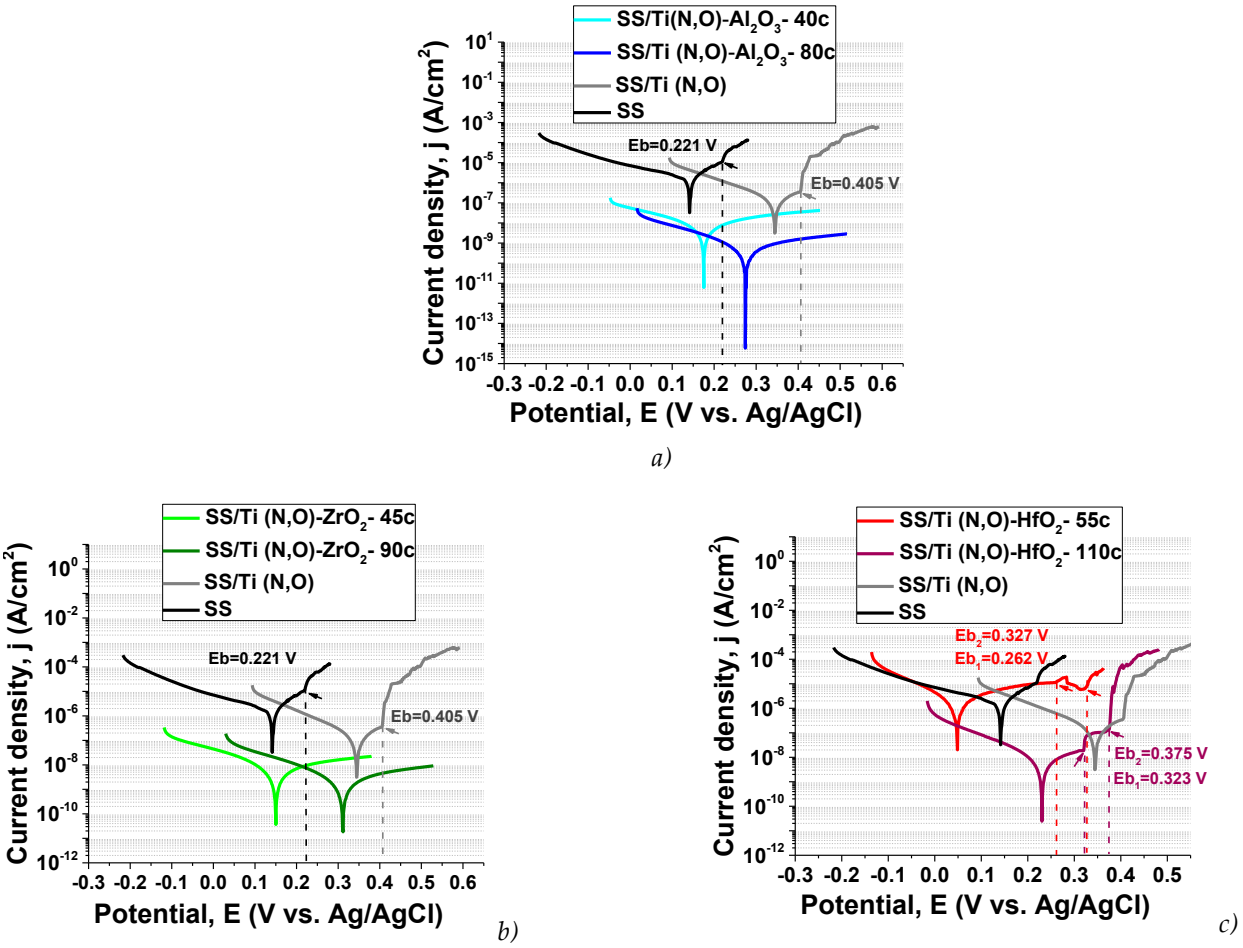

Figure 16. Tafel plots of oxides deposited on SS/Ti(N,O): a) Al_2O_3, b) ZrO_2 and c) HfO_2.

Table 2. Corrosion parameters (open circuit potential – E_{OC}, corrosion potential – E_{corr}, corrosion current density – i_{corr}, polarization resistance – Rp .

Sample	E_{OC} (mV)	E_{corr} (mV)	i_{corr} (nA/cm²)	βc (mV)	βa (mV)	Rp (kΩ)
SS	6	142	1,362	182.98	67.75	16
SS/Ti(N,O)	230	345	174	144.961	132.523	173
SS/Ti(N,O)-Al_2O_3-40c	190	171	12.6	240	509	5,627
SS/Ti(N,O)-Al_2O_3-80c	281	271	0.5	142	287	82,646
SS/Ti(N,O)-ZrO_2-45c	202	152	10.3	220	613	6,846
SS/Ti(N,O)-ZrO_2-90c	348	311	4.5	231	654	16,503
SS/Ti(N,O)-HfO_2-55c	83	48	4,344	185	428	13
SS/Ti(N,O)-HfO_2-110c	157	231	7.7	127	130	3627

The value of the open circuit potential (E_{oc}) depends on the chemical composition of the electrolyte, its temperature and oxygen content, as well as the nature of the investigated material [55=51], providing information about the sample's "nobility". All coatings presented more electropositive values compared to the SS support (Table 2), indicating a better corrosion resistance due to surface oxidation during the initial immersion in the electrolyte. The highest value was measured for SS/Ti(N,O)-ZrO_2-90c followed by SS/Ti(N,O)-Al_2O_3-80c.

A high electropositive corrosion potential value ($E_{i=0}$) is commonly admitted to indicate an improved resistance to corrosion. Using this criterion, one can observe that the samples coated with thicker oxide nano-layer were more resistant to corrosion attack than those with thinner oxide nano-layer.

Comparing the corrosion current density values (i_{corr}) we observed that the highest value was obtained for SS/Ti(N,O)-HfO_2-55c. All other coatings exhibited lower i_{corr} values than the bare SS support. This parameter is probably the most important in considering a material's corrosion resistance. In this respect, the samples coated with a thicker oxide nano-layer were more resistant to corrosion attack than those with a thinner oxide nano-layer, in the following order: SS/Ti(N,O)/Al_2O_3-80c>SS/Ti(N,O)/ZrO_2-90c> SS/Ti(N,O)/HfO_2-110c.

The polarization resistance (R_p) parameter designates the degree of protection imparted by the passive layer formed on the material's surface, such that a higher R_p value denotes a higher resistance to corrosive attack [56=52]. The R_p parameter has high values for SS/Ti(N,O)/Al2O_3-80c and SS/Ti(N,O)/ZrO_2-90c. Both hafnia top-coated samples show low values, in the following order: SS/Ti(N,O)/HfO_2-55c<SS<SS/Ti(N,O)< SS/Ti(N,O)/HfO_2-110c < SS/Ti(N,O)/Al_2O_3-40c.

For a comprehensive assessment related to the corrosion resistance of the samples we applied the Kendall rank correlation [57=53], considering the parameters with a major influence: E_{corr}, i_{corr} and R_p. Table 3 presents the results for each corrosion parameter labelled from 1 to 8, rank 1 being related to the best corrosion resistance, and rank 8 being assigned to the worst. The last column shows the sum of the ranks (ΣRanks) for each sample, and the best corrosion performance corresponds to the lowest Σranks value. Summing the ranks, we obtained the same values (4) for SS/Ti(N,O) and SS/Ti(N,O)-ZrO2-45c. The last column indicates the coatings' overall ranks. The coating ordering related to their corrosion resistance may be expressed as: SS/Ti(N,O)/Al_2O_3-80c > SS/Ti(N,O)/ZrO_2-90c > SS/Ti(N,O)/HfO_2-110c > SS/Ti(N,O)/ZrO_2-45c = SS/Ti(N,O) > SS/Ti(N,O)/Al_2O_3-40c > SS > SS/Ti(N,O)/HfO_2-55c. ~~Table 3 presents the results for each coating labelled in the following way: for each corrosion parameter the best results are ordered from 1 to 4, so rank 1 represents the best behaviour while rank 4 is assigned to the worst behaviour. In the last column the sum of the ranks (ΣRanks) for each sample are calculated, such that the highest corrosion performance corresponds to the lowest ΣRanks value.~~

Table 3. Kendall ranks attributed to the coated samples according to 3 corrosion parameters: corrosion potential – E_{corr}, corrosion current density – i_{corr}, polarization resistance – Rp.

Sample	Rank-E_{corr}	Rank-i_{corr}	Rank-R_p	ΣRanks	Overall Rank
SS	7	7	7	21	6
SS/Ti(N,O)	1	*6*	6	13	4
SS/Ti(N,O)-Al_2O_3-40c	5	5	4	14	5
SS/Ti(N,O)-Al_2O_3-80c	3	1	1	5	1
SS/Ti(N,O)-ZrO_2-45c	6	4	3	13	4
SS/Ti(N,O)-ZrO_2-90c	2	2	2	6	2
SS/Ti(N,O)-HfO_2-55c	8	8	8	24	7
SS/Ti(N,O)-HfO_2-110c	4	3	5	12	3

Summarizing, we conclude that the thicker ALD oxide coatings improved the corrosion resistance of the Ti(N,O) coated 304 L stainless steel. The best results were obtained when using alumina and zirconia as upper-coatings. Despite the quite high roughness of the coatings after corrosion, the coatings blocked the attack of the corrosive solution. The less promising results obtained for thin hafnia nano-layer coated samples might be related to thinner coating of HfO_2 than Al_2O_3 and ZrO_2 due to its lower growth rate, which is consistent with the hafnia composition shown in Table 1, pointing to a certain minimum thickness required for the ALD deposited oxide. This detail should be further studied, being probably a specific characteristic of each oxide.

4. Conclusions

We report on the deposition on stainless steel supports of two different layers with different compositions, Ti(N,O) oxynitride obtained by CAE and either alumina, or zirconia, or hafnia deposited by ALD. Though Ti(N,O) coated 304L stainless steel proved to be quite corrosion resistant in the applied ~~acidic,~~ saline and oxidising environment, the presence of some pinholes, specific for the cathodic arc evaporation still renders it vulnerable to oxidation and corrosion. This work aimed to increase the protection of the surface of Ti(N,O) coated 304L stainless steel in an aqueous ~~acidic,~~ saline and oxidizing solution by nanometer ultrathin Al_2O_3, ZrO_2, and HfO_2 ALD coatings. The corrosion protection behavior of the fabricated coatings was assessed by potentiodynamic polarization tests in simulated corrosive environment. The effect of the number of ALD cycles on ceramic film thickness and corrosion resistance were also investigated. Two thickness values of the oxides were deposited. The surfaces coated by oxynitride and oxides presented a good corrosion resistance, the best results being obtained for the thicker oxides, which outperformed the corrosion resistance of Ti(N,O) coated 304L stainless steel. The thicker Al_2O_3, ZrO_2, and HfO_2 ALD coatings with ~10nm thickness showed excellent corrosion resistance, while the thinner Al_2O_3, ZrO_2, and HfO_2 ALD coatings exhibited different performances. Thinner HfO_2 film had a lower corrosion resistance than Al_2O_3 and ZrO_2 film. The reason may come from different growth mechanism. The island growth mechanism of HfO_2 required more cycles of coating to efficiently protect the substrate. Due to the conformal nature of ALD coatings, the corrosion of droplets specific for the coatings obtained by cathodic arc evaporation could be efficiently contained, even with a thickness of only several nanometers, blocking the metal from interaction with the ~~acidic and~~ oxidizing environment.

The obtained results indicated that by CAE and ALD deposition methods can be obtained coatings with higher protection resistance to the corrosive attack in saline, acidic and oxidizing environment.

Author Contributions: Conceptualization, L.F.P. and V.B.; Methodology, M.B and X.L.; Validation, V.B., K.W.; Formal Analysis, M.B., X.L., Investigation, M.D., A.C.P., E.S.M.M., K.W.; Resources, V.B.,

X.L.; Data Curation, M.D, A.C.P, A.V., K.W.; Writing – Original Draft Preparation, E.S.M.M., M.D., M.D., K.W.; Supervision, L.F.P.; Writing-Review & Editing, M.B. and L.F.P.; Funding acquisition: M.B, L.F.P., X.L.; All authors reviewed and approved the work.

Funding: This work was carried out by the Core Program Project 18N/2019 and ~~granted by the Romanian Ministry for Research, Innovation and Digitization~~ through the Core Program within the National Research Development and Innovation Plan 2022-2027, carried out with the support of MCID, project no. PN 23 05 (M.D., A.C.P., V.B., A.V., M.B.); K.W. and X.L acknowledge the funding from US NSF award CBET-2306177 for the work in Washington University in St. Louis

Acknowledgments: A.V. thanks to Tomsk Polytechnic University within the framework of the Tomsk Polytechnic University-Competitiveness Enhancement Program grant; E.S.M.M. acknowledges Katri Laatikainen and Eveliina Repo from LUT for their support.

Conflicts of Interest: The authors declare no conflict of interest. The founding sponsors had no role in the design of the research; in the collection, analyses, or interpretation of data; in the writing of the manuscript, and in the decision to publish the results.

References

[1] Marin: E.; Guzman, L.; Lanzutti, A.; Fedrizzi, L.; Saikkonen, M., Chemical and electrochemical characterization of hybrid PVD+ALD hard coatings on tool steel, Electrochem. Commun. 11 (2009) 2060–2063, https://doi.org/10.1016/j.elecom.2009.08.052.

[2] Perillo, P.M., Corrosion Behavior of Coatings of Titanium Nitride and Titanium-Titanium Nitride on Steel Substrates, Corrosion. 62 (2006) 182–185, https://doi.org/10.5006/1.3278263.

[3] Subramanian, B.; Muraleedharan, C.V.; Ananthakumar, R.; Jayachandran, M., A comparative study of titanium nitride (TiN), titanium oxy nitride (TiON) and titanium aluminum nitride (TiAlN), as surface coatings for bio implants, Surf. Coatings Technol. 205 (2011) 5014–5020, https://doi.org/10.1016/j.surfcoat.2011.05.004.

[4] Chen, S.; Wu, B.H.; Xie, D.; Jiang, F.; Liu, J.; Sun, H.L.; Zhu, S.; Bai, B.; Leng, Y.X.; Huang, N.; Sun, H., The adhesion and corrosion resistance of Ti–O films on CoCrMo alloy fabricated by high power pulsed magnetron sputtering (HPPMS), Surf. Coatings Technol. 252 (2014) 8–14, https://doi.org/10.1016/j.surfcoat.2014.04.044.

[5] Pruncu, C.I.; Braic, M.; Dearn, K.D.; Farcau, C.; Watson, R.; Constantin, L.R.; Balaceanu, M.; Braic, V.; Vladescu, A., Corrosion and tribological performance of quasi-stoichiometric titanium containing carbo-nitride coatings, Arab. J. Chem. 10 (2017) 1015–1028, https://doi.org/10.1016/j.arabjc.2016.09.009.

[6] Braic, M.; Balaceanu, M.; Vladescu, A.; Kiss, A.; Braic, V.; Epurescu, G.; Dinescu, G.; Moldovan, A.; Birjega, R.; Dinescu, M., Preparation and characterization of titanium oxy-nitride thin films, Appl. Surf. Sci. 253 (2007) 8210–8214, https://doi.org/10.1016/j.apsusc.2007.02.179.

[7] Vitelaru, C.; Balaceanu, M.; Parau, A.; Luculescu, C.R.; Vladescu, A., Investigation of nanostructured TiSiC–Zr and TiSiC–Cr hard coatings for industrial applications, Surf. Coatings Technol. 251 (2014) 21–28, https://doi.org/10.1016/j.surfcoat.2014.04.001.

[8] Ma, F.; Li, J.; Zeng, Z.; Gao, Y., Structural, mechanical and tribocorrosion behaviour in artificial seawater of CrN/AlN nano-multilayer coatings on F690 steel substrates, Appl. Surf. Sci. 428 (2018) 404–414, https://doi.org/10.1016/j.apsusc.2017.09.166.

[9] Díaz, B.; Härkönen, E.; Światowska, J.; Maurice, V.; Seyeux, A.; Marcus, P.; Ritala, M., Low-temperature atomic layer deposition of Al_2O_3 thin coatings for corrosion protection of steel: Surface and electrochemical analysis, Corrosion Science 53 (2011) 2168-2175, https://doi.org/10.1016/j.corsci.2011.02.036.

[10] Zhang, C.; Yang, C.; Ding, G.; Wu, J., Effects of aging on the characteristics of TiNiPd shape memory alloy thin films, Mater. Charact. 59 (2008) 957–960, https://doi.org/10.1016/j.matchar.2007.08.013.

[11] Abbas, A.; Hung, H.-Y.; Lin, P.-C.; Yang, K.-C.; Chen, M.-C.; Lin, H.-C.; Han, Y.-Y., Atomic layer deposited TiO2 films on an equiatomic NiTi shape memory alloy for biomedical applications, J. Alloys Compd. 886 (2021) 161282, https://doi.org/10.1016/j.jallcom.2021.161282.

[12] Chu, C.L.; Chung, C.Y.; Lin, P.H., DSC study of the effect of aging temperature on the reverse martensitic transformation in porous Ni-rich NiTi shape memory alloy fabricated by combustion synthesis, Mater. Lett. 59 (2005) 404–407, https://doi.org/10.1016/j.matlet.2004.08.036.

[13] Baradaran, S.; Basirun, W.J.; Zalnezhad, E.; Hamdi, M.; Sarhan, A.A.D.; Alias, Y., Fabrication and deformation behaviour of multilayer Al2O3/Ti/TiO2 nanotube arrays, J. Mech. Behav. Biomed. Mater. 20 (2013) 272–282, https://doi.org/10.1016/j.jmbbm.2013.01.020.

[14] Bose, S.; Roy,M.; Bandyopadhyay, A., Recent advances in bone tissue engineering scaffolds, Trends Biotechnol. 30 (2012) 546–554, https://doi.org/10.1016/j.tibtech.2012.07.005.

[15] Zhang, H.; Marshall, C.L., Atomic layer deposition: Catalytic preparation and modification technique for the next generation, Chinese J. Catal. 40 (2019) 1311–1323, https://doi.org/10.1016/S1872-2067(19)63321-8.

[16] Marin, E.; Guzman, L.; Lanzutti, A.; Ensinger, W.; Fedrizzi, L., Multilayer Al_2O_3/TiO_2 Atomic Layer Deposition coatings for the corrosion protection of stainless steel, Thin Solid Films. 522 (2012) 283–288, https://doi.org/10.1016/j.tsf.2012.08.023.

[17] Peron, M.; Cogo, S.; Bjelland, M.; Bin Afif, A.; Dadlani, A.; Greggio, E.; Berto, F.; Torgersen, J., On the evaluation of ALD TiO_2, ZrO_2 and HfO_2 coatings on corrosion and cytotoxicity performances, J. Magnes. Alloy. 9 (2021) 1806–1819, https://doi.org/10.1016/j.jma.2021.03.010.
[18] Xu, Z.; Zhang, Q.; Luo, L.; Liu, Y.; Wan, J., Microstructure and corrosion resistance of TiN/TiO_2 nano-composite film on AZ31 magnesium alloy, Surf. Coatings Technol. 406 (2021) 126681, https://doi.org/10.1016/j.surfcoat.2020.126681.
[19] Shahmohammadi, M.; Sun, Y.; Yuan, J.C.-C.; Mathew, M.T.; Sukotjo, C.; Takoudis, C.G., In vitro corrosion behavior of coated Ti6Al4V with TiO_2, ZrO_2, and TiO_2/ZrO_2 mixed nanofilms using atomic layer deposition for dental implants, Surf. Coatings Technol. 444 (2022) 128686, https://doi.org/10.1016/j.surfcoat.2022.128686.
[20] Peron, M.; Bertolini, R.; Cogo, S., On the corrosion, stress corrosion and cytocompatibility performances of ALD TiO_2 and ZrO_2 coated magnesium alloys, J. Mech. Behav. Biomed. Mater. 125 (2022) 104945, https://doi.org/10.1016/j.jmbbm.2021.104945.
[21] Fedel, M.; Deflorian, F., Electrochemical characterization of atomic layer deposited Al_2O_3 coatings on AISI 316L stainless steel, Electrochim. Acta. 203 (2016) 404–415, https://doi.org/10.1016/j.electacta.2016.02.107.
[22] Díaz, B.; Światowska, J.; Maurice, V.; Seyeux, A.; Härkönen, E.; Ritala, M.; Tervakangas, S.; Kolehmainen, J.; Marcus, P., Tantalum oxide nanocoatings prepared by atomic layer and filtered cathodic arc deposition for corrosion protection of steel: Comparative surface and electrochemical analysis, Electrochim. Acta. 90 (2013) 232–245, https://doi.org/10.1016/j.electacta.2012.12.007.
[23] Daubert, J.S.; Hill, G.T.; Gotsch, H.N.; Gremaud, A.P.; Ovental, J.S.; Williams, P.S.; Oldham, C.J.; Parsons, G.N., Corrosion Protection of Copper Using Al_2O_3, TiO_2, ZnO, HfO_2, and ZrO_2 Atomic Layer Deposition, ACS Appl Mater Interfaces 9 (2017) 4192-4201, https://doi.org/10.1021/acsami.6b13571
[24] Gao, Y.; Walsh, M.; Liang, X., Atomic layer deposited conformal ceramic coatings for anti-corrosion of Ag 2anoparticles, Applied Surface Science 532 (2020), 147374, https://doi.org/10.1016/j.apsusc.2020.147374.
[25] Mondal, J.; Marques, A.; Aarik, L.; Kozlova, J.; Simões, A.; Sammelselg, V., Development of a thin ceramic-graphene nanolaminate coating for corrosion protection of stainless steel, Corrosion Science 105 (2016) 161-169, http://dx.doi.org/doi:10.1016/j.corsci.2016.01.013.
[26] Díaz, B.; Światowska, J.; Maurice, V.; Seyeux, A.; Normand, B.; Härkönen, E.; Ritala, M.; Marcus, P., Electrochemical and time-of-flight secondary ion mass spectrometry analysis of ultra-thin metal oxide (Al_2O_3 and Ta_2O_5) coatings deposited by atomic layer deposition on stainless steel, Electrochim. Acta. 56 (2011) 10516–10523, https://doi.org/10.1016/j.electacta.2011.02.074.
[27] Chai, Z.; Liu, Y.; Li, J.; Lu, X.; He, D., Ultra-thin Al_2O_3 films grown by atomic layer deposition for corrosion protection of copper, RSC Adv. 4 (2014) 50503-50509, https://doi.org/10.1039/c4ra09179e.
[28] Peron, M.; Cogo, S.; Bjelland, M.; Bin Afif, A.; Dadlani, A.; Greggio, E.; Berto, F.; Torgersen, J., On the evaluation of ALD TiO_2, ZrO_2 and HfO_2 coatings on corrosion and cytotoxicity performances, Journal of Magnesium and Alloys 2021, 9, 1806-1819, https://doi.org/10.1016/j.jma.2021.03.010.
[29] Behzadnasab, M.; Mirabedini, S.M.; Kabiri, K.; Jamali, S., Corrosion performance of epoxy coatings containing silane treated ZrO_2 nanoparticles on mild steel in 3.5% NaCl solution, Corrosion Science 53 (2011) 89-98, https://doi.org/10.1016/j.corsci.2010.09.026.
[30] Cai, Y.; Quan, X.; Li, G.; Gao, N., Anticorrosion and Scale Behaviors of Nanostructured ZrO_2–TiO_2 Coatings in Simulated Geothermal Water, Industrial & Engineering Chemistry Research 55 (2016) 11480-11494, https://doi.org/10.1021/acs.iecr.6b02920.
[31] Li, M.; Jin, Z.X.; Zhang, W.; Bai, Y.H.; Cao, Y.Q.; Li, W.M.; Wu, D.; Li, A.D., Comparison of chemical stability and corrosion resistance of group IV metal oxide films formed by thermal and plasma-enhanced atomic layer deposition, Sci. Rep. 9 (2019), 10438, https://doi.org/10.1038/s41598-019-47049-z.
[32] Staisiunas, L.; Kalinauskas, P.; Juzeliunas, E.; Griguceviciene, A.; Leinartas, K.; Niaura, G.; Stanionyte, S.; Selskis, A., Silicon Passivation by Ultrathin Hafnium Oxide Layer for Photoelectrochemical Applications, Front Chem 10 (2022) 859023, https://doi.org/10.3389/fchem.2022.859023.
[33] Park, S.W.; Han, G.D.; Choi, H.J.; Prinz, F.B.; Shim, J.H., Evaluation of atomic layer deposited alumina as a protective layer for domestic silver articles: Anti-corrosion test in artificial sweat, Appl. Surf. Sci. 441 (2018) 718–723, https://doi.org/10.1016/j.apsusc.2018.02.090.
[34] Boryło, P.; Lukaszkowicz, K.; Szindler, M.; Kubacki, J.; Balin, K.; Basiaga, M.; Szewczenko, J., Structure and properties of Al_2O_3 thin films deposited by ALD process, Vacuum. 131 (2016) 319–326, https://doi.org/10.1016/j.vacuum.2016.07.013.
[35] Mirhashemihaghighi, S.; Światowska, J.; Maurice, V.; Seyeux, A.; Klein, L.H.; Salmi, E.; Ritala, M.; Marcus, P., The role of surface preparation in corrosion protection of copper with nanometer-thick ALD alumina coatings, Appl. Surf. Sci. 387 (2016) 1054–1061, https://doi.org/10.1016/j.apsusc.2016.06.188.
[36] Li, J.; Pan, L.; Fu, Q.; Zhou, Y.; Guo, N., Wettability and corrosion behavior of a Ni coating on 304 stainless steel surface, Surf. Coatings Technol. 357 (2019) 740–747, https://doi.org/10.1016/j.surfcoat.2018.10.050.
[37]. Kuang, X.; Li, L.; Wang, L.; Li, G.; Huang, K.; Xu, Y., The effect of N_+ ion-implantation on the corrosion resistance of HiPIMS-TiN coatings sealed by ALD-layers, Surf. Coatings Technol. 374 (2019) 72–82, https://doi.org/10.1016/j.surfcoat.2019.05.055.
[38] Pana, I.; Braic, V.; Dinu, M.; Mouele, E.S.M.; Parau, A.C.; Petrik, L.F.; Braic, M., In Vitro Corrosion of Titanium Nitride and Oxynitride-Based Biocompatible Coatings Deposited on Stainless Steel, Coatings. 10 (2020) 710, https://doi.org/10.3390/coatings10080710.

[39] Bodunrin, M.O.; Chown, L.H.; van der Merwe, J.W.; Alaneme, K.K.; Oganbule, C.; Klenam, D.E.P; Mphasha, N.P., Corrosion behavior of titanium alloys in acidic and saline media: role of alloy design, passivation integrity, and electrolyte modification, Corros. Rev. 38/1 (2020) 25-47, https://doi.org/10.1515/corrrev-2019-0029.
[40] Seethammaraju, S; Rangarajan, M., Corrosion of stainless steels in acidic, neutral and alkaline saline media: Electrochemical and microscopic analysis, IOP Conf. Series: Materials Science and Engineering 577 (2019) 012188, doi:10.1088/1757-899X/577/1/012188.
[41] Dinu, M.; Parau, A.C.; Vladescu, A.; Kiss, A.E.; Pana, I.; Mouele, E.S.M.; Petrik, L.F.; Braic, V., Corrosion Improvement of 304L Stainless Steel by ZrSiN and ZrSi(N,O) Mono- and Double-Layers Prepared by Reactive Cathodic Arc Evaporation, Coatings 11/10 (2021) 1257, https://doi.org/10.3390/coatings11101257.
[40] Gao, Y.; Walsh, M.; Liang, X., Atomic layer deposited conformal ceramic coatings for anti-corrosion of Ag nanoparticles, Applied Surface Science, 532 (2020) 147374, doi: 10.1016/j.apsusc.2020.147374.
[43] Gorey, T.J.; Dai, Y.; Anderson, S.L.; Lee, S.; Lee, S.; Seifert, S.; Winans, R.E., Selective growth of Al_2O_3 on size-selected platinum clusters by atomic layer deposition, Surface Science 691 (2020): 121485, https://doi.org/ 10.1016/j.susc.2019.121485.
[44] Liu, J.; Li, J.; Wu, J.; Sun, J., Structure and dielectric property of high-k ZrO_2 films grown by atomic layer deposition using tetrakis (dimethylamido) zirconium and ozone, Nanoscale Research Letters 14/1 (2019) 1-12, https://doi.org/10.1186/s11671-019-2989-8.
[45] Gonta, C.J., Atomic Layer of Deposition of Ferroelectric HfO_2, Journal of the Microelectronic Engineering Conference, 23/1 (2017) 12, https://scholarworks.rit.edu/ritamec/vol23/iss1/12.
[46] Stern, M.; Geary, A.L., Electrochemical Polarization I. A theoretical analysis of the shape of polarization curves, J. Electrochem. Soc. 104 (1957) 56–63.
[47] Lebeau, B.; Naboulsi, I.; Michelin, L.; Marichal, C.; Rigolet, S.; Carteret, C.; Brunet, S.; Bonne, M.; Blin, J.L., Amorphous mesostructured zirconia with high (hydro)thermal stability, RSC Adv. 10 (2020) 26165-26176, https://doi.org/10.1039/D0RA04824K.
[48] Zhang, X.Y.; Hsu, C.H.; Lien, S.Y.; Wu, W.Y.; Ou, S.L.; Chen, S.Y.; Huang, W.; Zhu, W.Z.; Xiong, F.B.; Zhang, S., Nanoscale Temperature-Dependent HfO_2/Si Interface Structural Evolution and its Mechanism, Res. Lett. 14 (2019) 83, https://doi.org/10.1186/s11671-019-2915-0.
[49] Prokes, S. M.; Katz, M. B.; Twigg, M. E., Growth of crystalline Al_2O_3 via thermal atomic layer deposition: Nanomaterial phase stabilization, APL Materials 2 (2014) 032105, https://doi.org/10.1063/1.4868300.
[50] Miikkulainen, V.; Leskelä, M.; Ritala, M.; Puurunen, R.L., Crystallinity of inorganic films grown by atomic layer deposition: Overview and general trends, Journal of Applied Physics 113 (2013) 021301, https://doi.org/10.1063/1.4757907.
[51] Reclaru, L.; Eschler, P.Y.; Lerf, R.; Blatter, A., Electrochemical corrosion and metal ion release from Co-Cr-Mo prosthesis with titanium plasma spray coating, Biomaterials. 26 (2005) 4747–4756, https://doi.org/10.1016/j.biomaterials.2005.01.004.
[52 Baboian, R., Corrosion tests and standards: application and interpretation, ASTM Series, Philadelphia, USA, 2005.
[53] Kendall, M. G. Rank Correlation Methods; 2nd-nd ed.; Charles Griffin & Co.: London, 1955.